Highly Conductive and Strain-Released Hybrid Multilayer Ge/Ti Nanomembranes with Enhanced Lithium-Ion-Storage Capability

Chenglin Yan, Wang Xi,* Wenping Si, Junwen Deng, and Oliver G. Schmidt*

The demand for highly efficient lithium-ion batteries to power diverse electric devices is growing fast. Thus, the search for new electrode materials has become an urgent task in building next-generation lithium-ion batteries, so as to meet the ever-growing requirements for high capacity and high power density.[1–4] However, problems related to low electrical conductivity, large volume changes due to poor structural stability as well as high strain during repeated lithiation/delithiation processes have greatly hampered the application of electrode materials in lithium-ion batteries.[5–8] Hybrid micro-/nanostructures are a promising new class of materials due to their significant advantages over single-component systems.[9–12] Careful engineering of hybrid electrode materials providing both high storage capacity and high conductivity leads to enhanced Li storage properties.[13–16] Inspired by the above, we report here the fabrication of a promising, new type of hybrid configuration based on Ge/Ti multilayers, which results in electrode materials having very high capability and excellent capacity retention. Such a hybrid configuration, formed by strain release of Ge/Ti nanomembranes (herein nanomembranes are free-standing Ge/Ti film nanostructures) into tubular structures, allows us to achieve high conductivity and structural stability originating from a synergistic effect of clever materials combination. The choice of Ge as anode materials for lithium-ion batteries is due to its high theoretical Li^+ storage capacity of ≈1600 mA h g^{-1}, which is much larger than that (372 mA h g^{-1}) of graphite.[17,18] Another outstanding property of Ge is its high diffusion coefficient of Li^+, which is about two orders of magnitude higher than that in silicon, indicating that germanium can be an excellent candidate as high-performance anode materials.[17–20] Metallic Ti is employed mainly due to its outstanding electrical properties, high chemical stability and mechanical strength to prevent the pulverization of electrode materials.[21]

The large volume change of electrode materials due to a phase transformation from crystalline into amorphous structure during lithiation/delithiation processes could limit their use in high-capacity anodes for lithium-ion batteries.[22,23] Recently, Zachariah and co-workers suggested that amorphous materials are more effective than crystalline materials in narrowing the potential hysteresis and achieving faster conversion reaction rates.[24] Indeed, the strain in such amorphous structures can be relaxed easily without mechanical fracture. Maier and co-workers claimed that amorphization of RuO_2 could enhance the lithiation potential due to the enhanced Gibbs free energy in comparison to the crystalline RuO_2.[25] Moreover, diffusivity of Li ions in amorphous structures is much higher than that in the crystalline ones.[26] It is thus preferable to have an amorphous structure for good stability and high capacity performance due to the fact that the volume expansion of amorphous structures upon Li^+ insertion is homogeneous and causes less pulverization than that in crystalline materials.[27,28] Recently, Han and co-workers, designed a hierarchical porous structure of amorphous GeOx for lithium-ion batteries and achieved a very long-cycling life, which demonstrated the merits of porous structures in improving electrochemical performance.[29] In the present study, amorphous Ge and highly conductive Ti bilayer nanomembranes are combined to form hybrid multilayer microtubes by a strain release method, which reveals significantly improved electrochemical properties.

Nanomembranes consisting of a bilayer of two materials with different biaxial strains (β_1 and β_2) can roll-up into three-dimensional architectures if the built-in strain gradient over the bilayer is large enough ($\Delta\beta = \beta_2 - \beta_1 > 0.5\%$ estimated based on a bilayer model).[30,31] The whole process for the strain release of the Ge/Ti bilayer nanomembranes to form hybrid multilayer microtubes is schematically displayed in **Figure 1**.[32] Firstly, photoresist ARP 3510 as a sacrificial layer was spin-coated onto the substrates, then Ge and Ti were sequentially deposited onto the photoresist layer to form bilayer nanomembranes using electron beam deposition. The Ge/Ti nanomembranes bend and form a tubular structure after etching the sacrificial layer due to the existing intrinsic stress gradient in the bilayer.[31] The middle Ti multilayer will provide electron "superhighways" for charge storage and delivery because of its high electrical conductivity (Figure 1). Scanning electron microscopy (SEM) provides insight into the morphology and the detailed structure of the rolled-up microtubes. A panoramic view of the sample reveals that it is composed of uniform microtubes (**Figure 2**A). The obtained hybrid Ge/Ti microtubes feature two open ends, a smooth surface and a cylindrical hollow structure composed of multilayer stacks, which consist of periodically arranged Ge and Ti nanomembranes (Figure 2B). There are gaps that exist between the adjacent bilayers. They provide hollow channels

Dr. C. Yan, Dr. W. Xi, W. Si, J. Deng,
Prof. O. G. Schmidt
Institute for Integrative Nanosciences
IFW Dresden, Helmholtzstraße 20,
Dresden, 01069, Germany
E-mail: c.yan@ifw-dresden.de; w.xi@ifw-dresden.de
W. Si, J. Deng, Prof. O. G. Schmidt
Material Systems for Nanoelectronics
Chemnitz University of Technology
Straße der Nationen 62, Chemnitz, 09107, Germany

DOI: 10.1002/adma.201203458

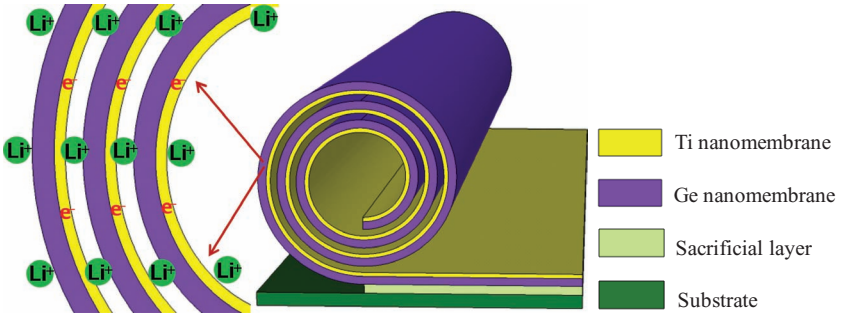

Figure 1. Schematic illustration of the rolled-up process of the hybrid Ge/Ti multilayer microtubes by the strain-released method: the middle Ti multilayer will provide electron "superhighways" for charge storage and delivery because of its high electrical conductivity. Nanomembranes consisting of a bilayer of Ge and Ti thin films can roll-up into three-dimensional architectures if the built-in strain gradient over the bilayer is larger than 0.5% ($\Delta\beta = \beta_2 - \beta_1 > 0.5\%$). β_1 and β_2 are the biaxial strains of the Ge and Ti films, respectively. The minimum strain gradient of 0.5% was estimated based on a bilayer model.

for electrochemical reaction and facilitate fast lithium-ion diffusion while also being the good tolerance for volume variation during charge/discharge. The formation of such gaps is due to the natural roughness of the deposited films, as well as the imperfect self-rolling process. Micro-Raman spectroscopy of a hybrid Ge/Ti microtube in comparison with a spectrum for crystalline Ge is shown in Figure 2C. Crystalline Ge usually has a characteristic phonon mode peak at ≈300 cm^{-1} while amorphous germanium typically exhibits a Raman spectrum peak at a lower wavenumber. Our germanium Raman spectra clearly show a red shift and a broadening peak, indicating the amorphous phase of the Ge. The formation of an amorphous structure of the Ge/Ti microtubes was also confirmed by X-ray diffraction data (Supporting Information, Figure S1). An SEM image (Figure 2D) and the corresponding energy-dispersive X-ray (EDX) spectroscopy for the separate elemental Ge and Ti mappings (Figure 2E,F) confirm the combination of Ge and Ti nanomembranes in the rolled-up wall of the hybrid microtubes.

The unique design of our hybrid multilayer Ge/Ti structures provides the following attractive features as an anode material. Firstly, the amorphous phase Ge microtubes with low conductivity, when incorporated into the Ti multilayers, exhibit a remarkably enhanced conductivity, which is more than two orders of magnitude higher than that of the pure Ge microtubes as confirmed by the conducting transport measurements on the single-microtube devices. Secondly, the incorporated Ti multilayers prevent the Ge tubular structures from collapsing

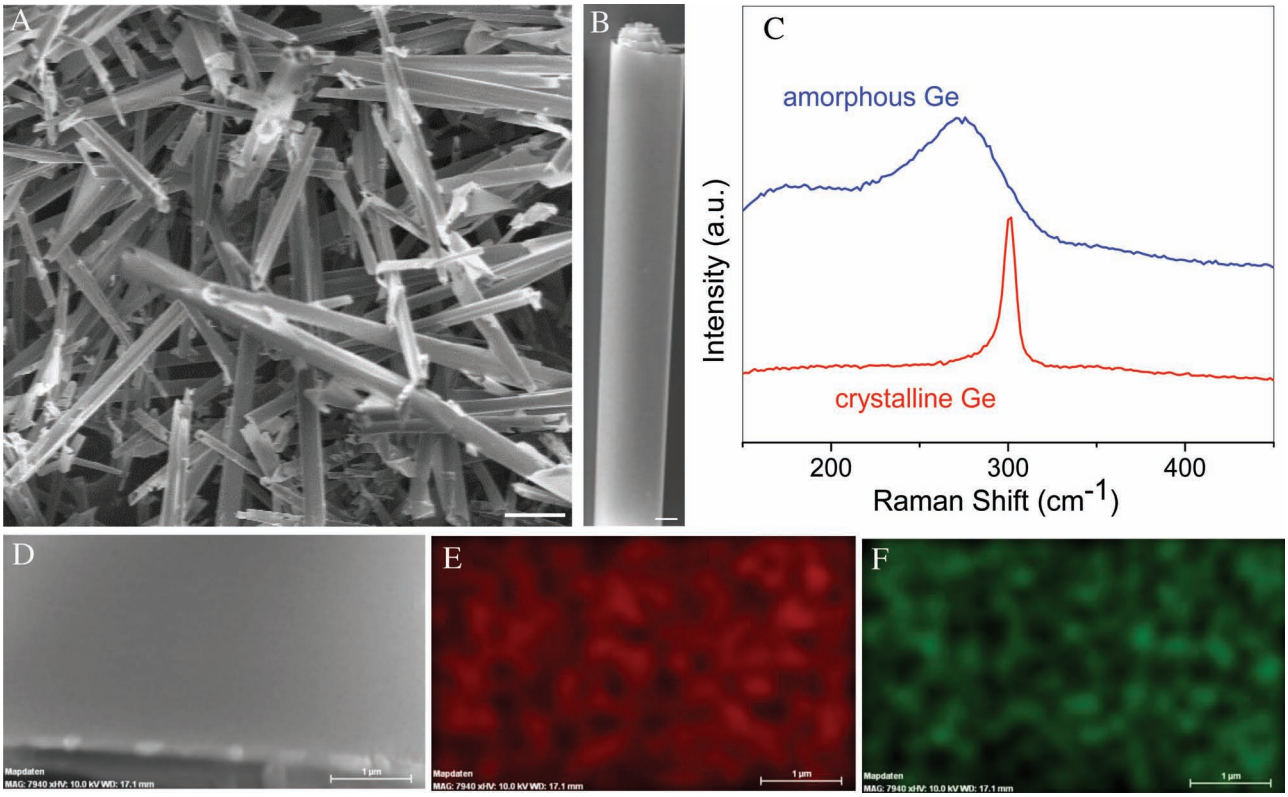

Figure 2. A) A typical SEM image of the hybrid multilayer Ge/Ti microtubes formed by the strain-released method, scale bar: 10 µm. B) A magnified SEM image of a single rolled-up Ge/Ti microtube showing a cylindrical hollow structure composed of multilayer stacks, scale bar: 2 µm. C) Micro-Raman spectra of a single hybrid Ge/Ti microtube and crystalline Ge as a reference. D–F) An SEM image (D) showing one opening of a microtube and the corresponding Ge (E) and Ti (F) elemental mapping images by EDX spectroscopy.

during the repeated lithiation/delithiation processes due to the high chemical stability and mechanical strength of metallic Ti. When lithium ions diffuse into the multilayer Ge/Ti tubes, the outer part of Ge is lithiated first and expands but is constrained by the inner part of Ti to maintain the initial structure. Thirdly, the amorphous nature of the strain-released Ge microtubes enables homogenous volume expansion and contraction, which are further buffered by the inner hollow space of the microtubes. Moreover, the tubular morphology offers a unique combination of large area surface and low internal resistance. Therefore, in this hybrid electrode design, not only are all the desired functions of each constituent effectively utilized, but additionally a synergistic effect can be realized.

Electrochemical experiments were performed to evaluate the charge/discharge performance of the microtubes. In the first cycle, the hybrid Ge/Ti electrodes are able to exhibit a high first-cycle Coulombic efficiency (**Figure 3**A,B), in contrast to a large irreversible capacity loss usually observed in the first cycle for most of previously reported Ge micro-/nanostructured electrodes. The capacity was calculated based on the total mass of the hybrid Ge/Ti microtubes composed of 94% of Ge and 6% of Ti. The discharge (lithiation) and charge (delithiation) capacities of the hybrid Ge/Ti microtubes are 1753 mA h g^{-1} and 1490 mA h g^{-1}, respectively, corresponding to a first-cycle efficiency of 85%, which is higher than those for Ge nanowire arrays (33%),[33] Ge nanotubes (76%)[34] and Ge/graphene composites (52%).[35] Clearly, the presence of multiple Ti layers significantly improves the Coulombic efficiency for the first cycle, providing a high reversible capacity.

Notably, in the continuous charge/discharge experiments the hybrid Ge/Ti electrode shows a first reversible discharge capacity as high as 1495 mA h g^{-1} at a constant current density of C/16 (Figure 3A). Even crystalline Ge/graphene composites cannot match such a capacity,[35] while the pure Ge microtube electrode without Ti incorporation only delivers a low reversible capacity of 1097 mA h g^{-1}. In comparison with other Ge based nanostructures, such as Ge nanoparticles[36] and Ge/C nanocomposites,[35] the reversible capacity of the pure Ge microtubes is still higher even after 100 cycles, demonstrating the advantages of the strain-released structures in improving electrochemical properties and enhancing cycling performance (Figure 3A). Moreover, after 100 cycles the hybrid Ge/Ti microtubes exhibit excellent capacity retention and maintain a stable capacity of ≈930 mA h g^{-1} with a high Coulombic efficiency (Figure 3B), which is about 3 times higher than the theoretical maximum capacity of graphite. However, the specific capacity of the pure Ge microtubes drops to a relatively low value of ≈600 mA h g^{-1}. As pointed out before, the main reason for rapid fading of Ge electrodes is that a large volume expansion of the material occurs during the cycling, leading to the pulverization of the electrodes. The roll-up of the

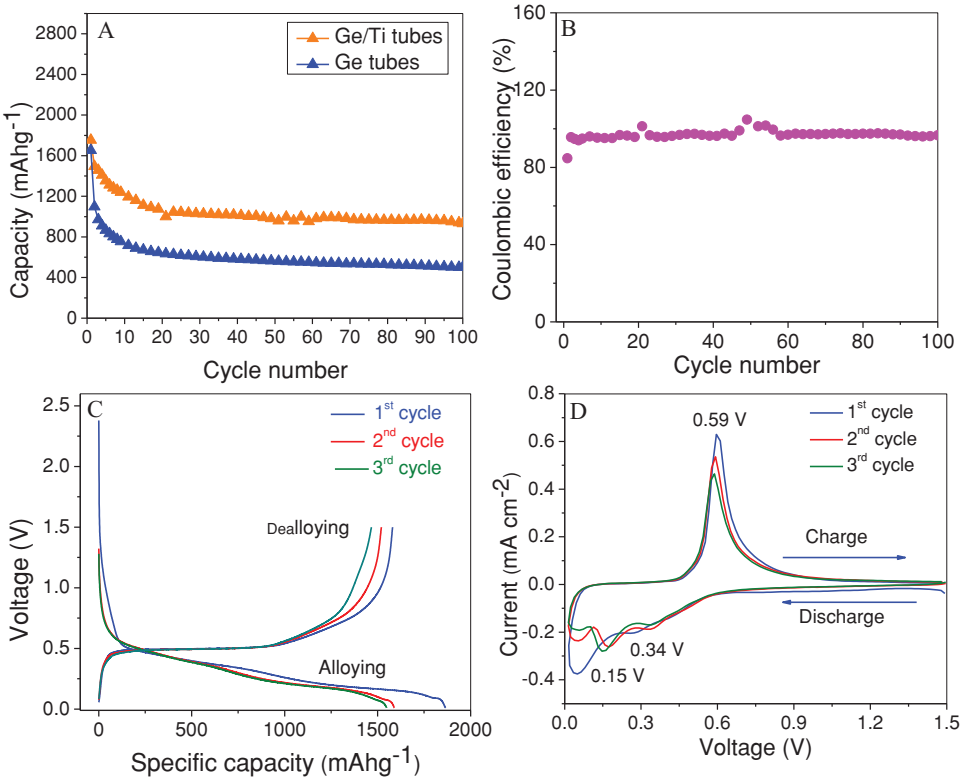

Figure 3. Electrochemical characterizations for the hybrid Ge/Ti and Ge microtubes as positive electrodes in lithium-ion batteries. A) Comparative cycling performance showing the discharge capacities of the hybrid Ge/Ti and pure Ge microtubes at a current rate of C/16 from 0.05 V to 1.5 V versus Li/Li^+. The capacity was calculated based on the total mass of the hybrid Ge/Ti or Ge microtubes. B) Coulombic efficiency of the hybrid Ge/Ti microtubes at different cycles. C) Charge-discharge voltage profiles for the hybrid Ge/Ti multilayer microtubes cycled at a rate of C/16 between 1.5 and 0.01 V versus Li/Li^+. D) Cyclic voltammogram for the hybrid Ge/Ti microtubes from 1.5 V to 0.05 V versus Li/Li^+ at a 0.1 mV s^{-1} scan rate: the first three cycles are shown.

strained thin films into microtube electrodes is driven by the minimization of the total elastic energy, resulting in a reduced strain during the charge and discharge processes, improving the capacity and cycling performance.

We expect that the use of Ti multilayers as efficient electron pathways to enhance surface electrochemical reactivity will lead to further improvements in the rate capability. After 100 cycles the same battery was further evaluated for rate capability as shown in the Supporting Information. The hybrid Ge/Ti microtube electrode shows a much higher capacity than the pure Ge microtubes under all investigated current densities. The specific capacities of the hybrid anode at the discharge rates of C/16 and C/2 are found to be 930 mA h g^{-1} and 565 mA h g^{-1} (Supporting Information, Figure S2), respectively, which are higher than those of the pure Ge microtubes at the same current rates (Supporting Information, Figure S3). By returning to the initial rate of C/16, the hybrid electrodes regain the original capacity of ≈915 mA h g^{-1} (Supporting Information, Figure S4), and continues to operate with a stable cycling response. For the same specific current rate (C/16), the pure Ge electrodes show only a very low capacity of ≈480 mA h g^{-1}. Clearly, the hybrid Ge/Ti microtube electrode possesses a high electrical conductivity, resulting in a better rate capability in comparison with the pure Ge microtubes.

To understand the cycling performance further, we used SEM to examine the morphology evolution of the microtubes before and after lithiation. Before lithiation the microtubes show a smooth surface (Supporting Information, Figure S5A). After the first cycle the surface of the microtubes becomes rough (Supporting Information, Figure S5B). SEM images of the electrodes after 100 cycles are also examined, and the tubular structure is conspicuously maintained, although there exists a change in the size, perhaps due to solid electrolyte interphase (SEI) formation and the volume change of the microtubes (Supporting Information, Figure S5C). The above results indicate the enhanced structural stability of the rolled-up microtubes during lithiation/delithiation, which leads to the improved electrochemical performance of the Ge/Ti microtubes.

The voltage profile with different flat plateaus due to the redox reactions associated with Li^+ insertion/extraction can be observed in the first discharge and charge curves (Figure 3C). The electrochemical reaction of Li^+ with Ge has been shown to follow the equilibrium Li-Ge phase diagram and therefore displays the distinct voltage plateaus (mostly notably at ≈0.5 V during discharge), indicating the formation of new phases. These redox reactions can be clearly illustrated using cyclic voltammetry (CV). Figure 3D shows typical CV curves of the hybrid Ge/Ti microtube electrode in the 0.01–1.5 V versus Li/Li^+ potential window at a scan rate of 0.1 mV s^{-1}. The reduction peaks of the first discharge can be assigned to the successive phase transformations upon lithium-ion insertion via Ge to form different Li/Ge alloys.[37] Two distinct peaks at about 0.05 V and 0.28 V appear in the first reverse anodic scan, but they disappear during further cycles while new well-defined peaks at about 0.15 and 0.34 appear, which are attributed to the phase transition between lithiated Li_xGe and amorphous Ge. On the other hand, the absence of a peak at around 0.6 V in the anodic scan corresponding to the irreversible lithiation during the first cycle indicates the side reaction can be substantially reduced, which is usually associated with the formation of SEI during the first discharge. Additionally, a very large and sharp peak at ≈0.59 V is observed during the first charge, which is shifted to lower voltage after further cycles. This behavior of voltage–capacity curves (Figure 3C) for the hybrid Ge/Ti electrodes is similar to that of Ge nanoparticles produced by other methods.[37]

To understand the superior performance of the hybrid multilayer Ge/Ti microtubes for Li^+ storage, a single-microtube-based lithium-ion battery device was fabricated for in situ probing the direct correlation of the electrical transport and electrochemistry properties in order to eliminate any artifacts originating from the binders or conductive additives. The strain-release method provides a straightforward and novel way to establish reliable and gentle contacts, allowing us to overcome limitations apparent in conventional lithography. Specifically, the gold finger contacts were first patterned on the substrate, which consists of Cr/Au (3/50 nm) layers deposited by thermal evaporation. The device fabrication starts with the fabrication of a planar strained multilayer nanomembrane by the sequential deposition of Ge and Ti thin films on top of a sacrificial layer (**Figure 4**A). Once the sacrificial layer is selectively removed, the strained Ge/Ti bilayer starts to roll towards the Au finger structures. After the rolling process the rolled-up microtube rests on top of the Au fingers establishing an electrical connection (Figure 4B, see Supporting Information, Figure S6 for more details). The thickness of the Ge nanomembrane has to be carefully designed to provide the necessary strain to force the roll-up of the nanomembrane, while to keep the formed Ge/Ti microtube fixed to the substrate. We stress that the fixing of a single microtube onto a substrate is quite useful in the accurate positioning and integration of single-microtube devices for on-chip electronic applications. The diameter of the rolled-up Ge/Ti microtube can be precisely controlled and calculated using a macroscopic continuum mechanical model,[38] expressed by Equation 1, which is given by:

$$D_0 = \frac{d_2}{3[(1+\upsilon_2)\varepsilon_2(1+\upsilon_1)\varepsilon_1}\frac{1+4\rho\delta+6\rho\delta^2+4\rho\delta^3+\rho^2\delta^4}{\rho\delta(1+\delta)} \quad (1)$$

where D_0 is the outer tubular diameter, the thickness ratio is given by $\delta = d_1/d_2$, where d_1 and d_2 are the layer thicknesses of Ge and Ti, respectively. υ_1 and υ_2 are the Poisson's ratio of Ge and Ti, respectively. ε_1 and ε_2 are the inplane biaxial strains of the Ge and Ti layers, respectively. The Young's modulus ratio is expressed by $\rho = Y_1/Y_2$, where Y_1 and Y_2 are the Young's moduli of Ge and Ti, respectively. Based on the above equation, the diameter of the rolled-up Ge/Ti microtubes can thus be estimated to be 25.0 μm with 40 nm Ge and 3 nm Ti layers deposition, which agrees very well with our experimentally measured results, and a linear relation between the thickness and the diameter can be obtained (Supporting Information, Figure S7).

Figure 4C shows a single rolled-up device for electric transport measurements during lithiation and delithiation. The middle electrode acts as the anode for the lithium-ion battery and the two electrodes at the open ends are used for electrical transport measurements. In the experiments, a single rolled-up Ge/Ti microtube is used as the working electrode, propylene carbonate/ethylene carbonate acts as the electrolyte, while a metallic lithium foil serves as the counter electrode

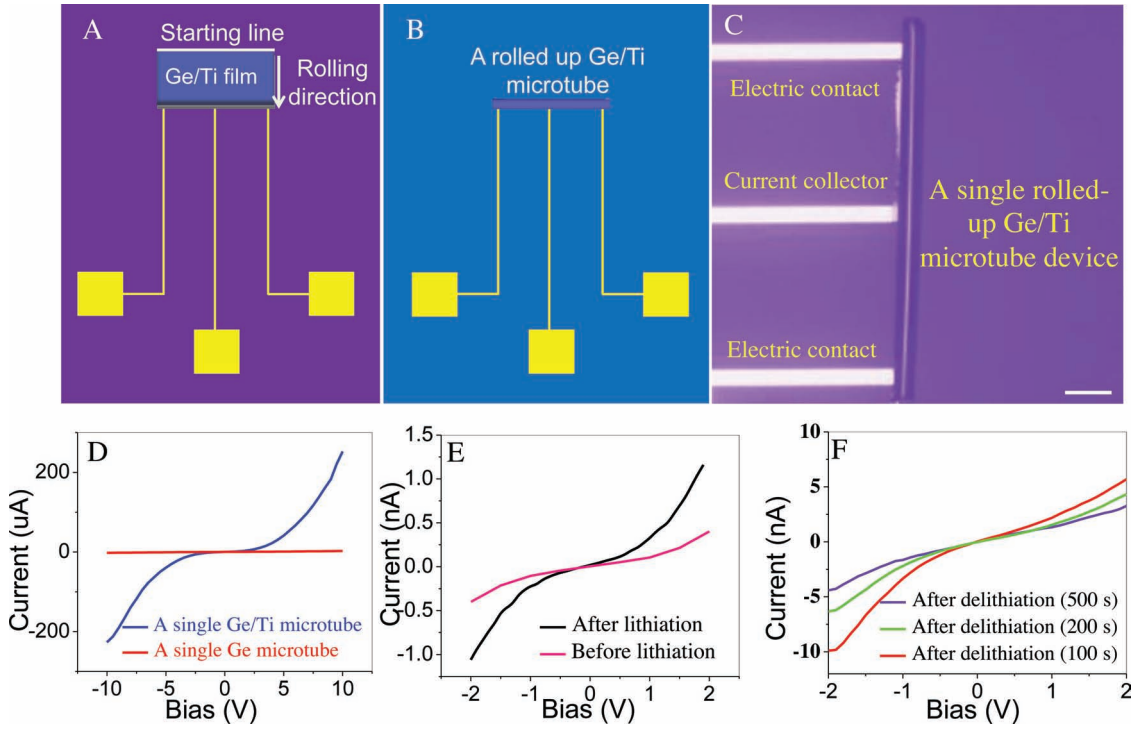

Figure 4. A,B) A schematic of the single-microtube-device fabrication showing the planar device before rolling (left) and the device after rolling the Ge/Ti nanomembranes (right). The strained bilayer consists of the Ge and Ti nanomembranes patterned on top of a sacrificial layer. Once the sacrificial layer is selectively removed, the strained Ge/Ti bilayer starts to roll toward the Au finger structures. After the rolling process, the rolled-up microtube rests on top of the Au fingers establishing an electrical connection. C) An optical microscopy overview image of a single rolled-up device after the selective removal of the sacrificial layer; the transport measurements on single rolled-up microtubes were conducted by connecting two end contacts, while the middle contact is used as a current collector for the electrochemical measurements; scare bar: 50 µm. D) Transport properties of the single Ge/Ti and Ge microtubes. E) Transport properties of a single Ge/Ti microtube before discharge (red curve) after discharge at 2 nA for 400 s (black curve). F) The transport properties after charge for 100 s (red curve), 200 s (green curve), and 500 s violet curve.

(Supporting Information, Figure S8,S9). We have conducted an electrical transport investigation on a single Ge/Ti microtube before and after lithiation. Before lithiation, current–voltage (*I–V*) curves of the hybrid Ge/Ti and pure Ge microtubes at 298 K are measured and shown in Figure 4D. The hybrid Ge/Ti structure exhibits a very high electric conductivity of 2.38×10^{-2} S cm^{-1}, compared to a conductivity of 1.28×10^{-4} S cm^{-1} for a pure Ge microtube, highlighting the merits of the incorporation of multilayer Ti in significantly improving the conductivity. After lithiation, the electrochemical insertion of Li atoms into the amorphous Ge results in an increase in the conductivity (Figure 4E). This enhancement of the conductivity performance by almost one order of magnitude is due to the insertion of lithium into the amorphous Ge microtubes and the formation of more conductive Li_xGe alloys. Indeed, during lithiation the Li atoms at the surface gradually move into the amorphous Ge by breaking the Ge-Ge bonds, which allows the amorphous Ge to expand in order to accommodate them. In the meantime several local structures such as single-phase regions where the amorphous Ge is lithiated, and a succession of amorphous Li_xGe and finally crystalline Li-Ge phases like $Li_{15}Ge_4$ will be formed. The formed Li_xGe alloy during the Li insertion is a doped semiconductor and the Li_xGe alloy might also exhibit metallic properties, which can explain the conductivity enhancement. However, after delithiation (lithium leaves the host Ge material), a decrease in the conductivity was measured and the conductivity of the hybrid Ge/Ti can be partially recovered (Figure 4F). The conductivity continuously decreased along with electrochemical cycling after charging with 2 nA for 100 s (red curve), 200 s (green curve) and 500 s (violet curve) (Figure 4F), which is attributed to the decomposition of the conductive Li_xGe alloy and the formation of the less-conductive Ge. Such conductivity increase during lithiation and decrease during delithiation demonstrates the reversible phase and structure changes of the hybrid Ge/Ti multilayer microtube during discharge/charge processes.

In summary, we have fabricated a novel hybrid structure composed of multilayer Ge and Ti nanomembranes by using a strain release method. The unique hybridization of the highly conductive Ti/Ge nanomembranes offers enhanced electronic transport and rigid frames to stabilize the structures, leading to better reversible capacity and excellent cycling performance. The intrinsic strain accommodated in the Ge/Ti bilayer nanomembranes is efficiently released by a self-rolling process that thus offers a minimization of the whole system energy. To explain the outstanding charge and discharge performance of the hybrid Ge/Ti composites, we conducted electric transport measurements on single microtubes before and after lithiation, revealing the structure flexibility of the hybrid structures and addressing fundamental questions related to the transport

behavior in single-microtube energy-storage devices. We stress that the ease of fabrication of single rolled-up microtubes on semiconductor substrates makes them more suitable for lab-on-chip microbattery applications as well as microintegration with other electronic devices. The proof-of-concept of the material combination and structural design presented in this work combining top-down and bottom-up approaches should be valuable for the preparation of other electrode materials of various combinations for future high-performance lithium-ion batteries.

Experimental Section

Preparation of the Hybrid Multilayer Ge/Ti Microtubes: An ARP-3510 photoresist as a sacrificial layer was spin-coated on the Si substrates at 3500 rpm prior to baking at 90 °C for 5 min on a hot plate. Then, 40 nm Ge and 3 nm Ti nanomembranes were sequentially deposited onto the sacrificial layer using electron-beam deposition. After deposition, the sample was directly immersed into acetone for the rolling process. Acetone was used for the etching process to release the Ge/Ti nanomembranes, leading to the formation of the hybrid multilayer Ge/Ti microtubes. The microstructure and chemical composition of the samples were investigated using a field-emission scanning electron microscope (JEOL JSM 6400, 15 keV) equipped with an energy-dispersive X-ray (EDX) spectroscopy instrument, a scanning electron microscope (DSM 982 Gemini, Carl Zeiss, Oberkochen, Germany) with a 5 keV acceleration voltage, and InVia photoluminescence/Raman microscopes (Renishaw) with an excitation line at 442 nm. The transport properties were investigated using a Keithley series 2612A measurement system.

The electrochemical properties were studied with a multichannel battery-testing system (Arbin BT 2000). Lithium-ion batteries were fabricated using a lithium foil as the negative electrode, 1.0 M solution of $LiPF_6$ in ethylene carbon (EC)/dimethyl carbonate (DMC) as the electrolyte, and a pellet made of the hybrid Ge/Ti microtubes, carbon black, and *N*-methyl-2-pyrrolidone (NMP) in a 7:2:1 ratio as the positive electrode. The capacity was calculated based on the total mass of the hybrid Ge/Ti microtubes composed of 94% of Ge and 6% of Ti. The evaluation of the mass ratio of the germanium/titanium was calculated from the thicknesses of the films, the surface area, and the densities of Ge ($d_{Ge} = 5.3$ g cm^{-3}) and Ti ($d_{Ti} = 4.5$ g cm^{-3}). Lithium-ion batteries were prepared within an argon-filled glove box using a Cu foil current collector, which were charged and discharged galvanostatically between 1.5 and 0.01 V versus Li/Li$^+$. The cyclic voltammetry test was performed between 0.05 and 1.5 V versus Li/Li$^+$ at a scanning rate of 0.1 mV s^{-1} via a Zahner electrochemical workstation (IM6ex) using the active anode as the working electrode and lithium as both the counter and reference electrodes.

Supporting Information

Supporting Information is available from the Wiley Online Library or from the author.

Acknowledgements

This work was financed by the International Research Training Group (IRTG) project, the pakt project "Electrochemical energy storage in autonomous systems, Nr. 49004401", and the Volkswagen Foundation (86 362). We express our thanks to Kaikai Song at IFW Dresden for his strong support.

Received: August 20, 2012
Revised: September 19, 2012
Published online: October 26, 2012

[1] J. M. Tarascon, M. Armand, *Nature* **2001**, *414*, 359.
[2] J. B. Goodenough, K. Youngsik, *Chem. Mater.* **2010**, *22*, 587.
[3] J. M. Tarascon, M. Armand, *Nature* **2001**, *414*, 359.
[4] Z. Y. Wang, L. Zhou, X. W. Lou, *Adv. Mater.* **2012**, *24*, 1903.
[5] K. T. Nam, D. W. Kim, P. J. Yoo, C. Y. Chiang, N. Meethong, P. T. Hammond, Y. M. Chiang, A. M. Belcher, *Science* **2006**, *312*, 885.
[6] A. S. Arico, P. Bruce, B. Scrosati, J. M. Tarascon, W. Van Schalkwijk, *Nat. Mater.* **2005**, *4*, 366.
[7] S. Yang, X. Feng, S. Ivanovici, K. Müllen, *Angew. Chem., Int. Ed.* **2010**, *49*, 8408.
[8] M. S. Whittingham, *Chem. Rev.* **2004**, *104*, 4271.
[9] C. Yan, A. Dadvand, F. Rosei, D. F. Perepichka, *J. Am. Chem. Soc.* **2010**, *132*, 8868.
[10] C. Yan, L. Nikolova, A. Dadvand, C. Harnagea, A. Sarkissian, D. F. Perepichka, D. F. Xue, F. Rosei, *Adv. Mater.* **2010**, *22*, 1741.
[11] C. C. Bof Bufon, J. D. Arias Espinoza, D. J. Thurmer, M. Bauer, C. Deneke, U. Zschieschang, H. Klauk, O. G. Schmidt, *Nano Lett.* **2011**, *11*, 3727.
[12] Y. Y. Liang, Y. G. Li, H. L. Wang, J. G. Zhou, J. Wang, T. Regier, H. J. Dai, *Nat. Mater.* **2011**, *10*, 780.
[13] H. X. Ji, X. L. Wu, L. Z. Fan, C. Krien, I. Fiering, Y. G. Guo, Y. F. Mei, O. G. Schmidt, *Adv. Mater.* **2010**, *22*, 4591.
[14] C. C. Bof Bufon, J. D. C. Gonzlez, D. J. Thurmer, D. Grimm, M. Bauer, O. G. Schmidt, *Nano Lett.* **2010**, *10*, 2506.
[15] A. L. M. Reddy, M. M. Shaijumon, S. R. Gowda, P. M. Ajayan, *Nano Lett.* **2009**, *9*, 1002.
[16] W. Wang, M. Tian, A. Abdulagatov, S. M. George, Y. C. Lee, R. G. Yang, *Nano Lett.* **2012**, *12*, 655.
[17] M. H. Seo, M. Park, K. T. Lee, K. Kim, J. Kim, J. Cho, *Energy Environ. Sci.* **2011**, *4*, 425.
[18] M. H. Park, K. Kim, J. Kim, J. Cho, *Adv. Mater.* **2010**, *22*, 415.
[19] J. Graetz, C. C. Ahn, R. Yazami, B. Fultz, *J. Electrochem. Soc.* **2004**, *151*, A698.
[20] G. Cui, L. Gu, L. Zhi, N. Kaskhedikar, P. A. van Aken, K. Müllen, J. Maier, *Adv. Mater.* **2008**, *20*, 3079.
[21] F. Variola, F. Vetrone, L. Richert, P. Jedrzejowski, J. H. Yi, S. Zalzal, S. Clair, A. Sarkissian, D. F. Perepichka, J. D. Wuest, F. Rosei, A. Nanci, *Small* **2009**, *5*, 996.
[22] L. F. Cui, R. Ruffo, C. K. Chan, H. L. Peng, Y. Cui, *Nano Lett.* **2009**, *9*, 491.
[23] S. Ohara, J. J. Suzuki, K. Sekine, T. Takamura, *Electrochemistry* **2003**, *71*, 1126.
[24] J. C. Guo, Q. Liu, C. S. Wang, M. R. Zachariah, *Adv. Funct. Mater.* **2012**, *22*, 803.
[25] O. Delmer, P. Balaya, L. Kienle, J. Maier, *Adv. Mater.* **2008**, *20*, 501.
[26] H. Ghassemi, M. Au, N. Chen, P. A. Heiden, R. S. Yassar, *ACS Nano* **2011**, *5*, 7850.
[27] J. T. Yin, M. Wada, K. Yamamoto, Y. Kitano, S. Tanase, T. Sakai, *J. Electrochem. Soc.* **2006**, *153*, A472.
[28] L. Y. Beaulieu, K. W. Eberman, R. L. Turner, L. J. Krause, J. R. Dahn, *Electrochem. Solid State Lett.* **2001**, *4*, A137.
[29] X. L. Wang, W. Q. Han, H. Chen, J. Bai, T. A. Tyson, X. Q. Yu, X. J. Wang, X. Q. Yang, *J. Am. Chem. Soc.* **2011**, *133*, 20692.
[30] G. P. Nikishkov, *J. Appl. Phys.* **2003**, *94*, 5333.
[31] O. G. Schmidt, K. Eberl, *Nature* **2001**, *410*, 168.
[32] Y. F. Mei, G. S. Huang, A. A. Solovev, E. Bermúdez Ureña, I. Moench, F. Ding, T. Reindl, R. Fu, P. K. Chu, O. G. Schmidt, *Adv. Mater.* **2008**, *20*, 4085.
[33] C. K. Chan, X. F. Zhang, Y. Cui, *Nano Lett.* **2008**, *8*, 307.
[34] M. H. Park, Y. Cho, K. Kim, J. Kim, M. Liu, J. Cho, *Angew. Chem., Int. Ed.* **2011**, *123*, 9821.
[35] D. J. Xue, S. Xin, Y. Yan, K. C. Jiang, Y. X. Yin, Y. G. Guo, L. J. Wan, *J. Am. Chem. Soc.* **2012**, *134*, 2512.
[36] J. S. Cheng, J. Du, *CrystEngComm* **2012**, *14*, 397.
[37] B. Laforge, L. L. Jodin, R. Salot, A. Billard, *J. Electrochem. Soc.* **2008**, *155*, A181.
[38] G. P. Nikishkov, *J. Appl. Phys.* **2003**, *94*, 5333.